Gain Enhanced Characteristics of Miniaturized Antenna for 5 GHz WLAN Application

Kakani Suvarna[1, *], Nallagarla Ramamurthy[2], and Dupakuntla V. Vardhan[1]

Abstract—In this article, a miniaturized pentagonal slot antenna (PSA) with a Meander Koch Defected Ground Structures (MK-DGS) and metamaterials (MTM) is proposed for 5 GHz WLAN application. Initially, a Meander Koch DGS was used to lower the resonant frequency of the basic PSA, from 13.1 GHz to 5 GHz. The proposed antenna has been 61.83% miniaturized, close to an electrically small antenna. The performance characteristics of a basic PSA using MK-DGS and MTM superstrate, which improves efficiency, directivity, and peak gain, are also discussed. An antenna with dimensions of $15 \times 15 \, \text{mm}^2$ (or) $0.25\lambda_0 \times 0.25\lambda_0 \, \text{mm}^2$ at a thickness of $h_1 = 1.6 \, \text{mm}$ is designed, fabricated, and tested on an FR4 epoxy substrate, and its impact on size reduction performance is evaluated. The gain at 5 GHz is increased from 3.15 to 7.84 dBi by introducing an MTM superstrate made of RT Duriod at a thickness of 1.575 mm above the miniaturized PSA at 17 mm. Test results of the prototype model are corroborated by the simulated results of the proposed model.

1. INTRODUCTION

A small wireless transceiver is necessary for portable wireless devices. Most RF transceivers are characterized by large antennas with the largest amount of space. Therefore, RF designers strive to minimize the size of their antennas. Miniaturized antennas are in high demand today in order to meet the demanding specifications of modern wireless communication systems. Fallahpour and Zoughi [1] suggested that modified meander line, Koch fractal, and metamaterial-inspired designs are the most commonly used techniques for antenna miniaturization. Spherical mode radiating fields were mentioned by Chu [2]. The concept of "an electrically small antenna" is similar to that of reducing the size of antennas with $Ka \leq 1.0$. 'K' corresponds to the vector of wave propagation ($K = 2\pi/\lambda$), and 'a' represents the radius of a sphere which encircles the antenna [3]. Erentok and Ziolkowski explained about the radiation characteristic that indicates a reduction in impedance-bandwidth, peak gain, and quality factor (Q) for the design of compact antennas [4]. Resonators with a helical μ-negative (MNG) structure for miniaturized antennas were investigated by Jahani et al. [5]. There have been several miniaturization methods developed for planar and non-planar slot antennas, including slits, strips, wires, and loops loading techniques [6–9]. Various antenna designs are used in reductions in size methods based on Complimentary Spilt Ring Resonator (CSRR), Fractal Electromagnetic Band Gap (FEBG), Spilt Ring Resonator (SRR), and Single Spilt Ring Resonator (SSRR) structure [10–12]. Mishra and Chaudhary [13] investigated an electric LC resonator-based MTM miniaturized antenna with a high gain. DGS was used to decrease the size of the patch and its array components [14–19]. Antennas designed with superstrate configurations have improved gain and directivity [20, 21].

This article outlines two miniaturization methods: one with antenna size and the other with switching resonant frequency. The Chu-limit is satisfied by electrically small antenna with a miniaturization of 61.83%. The idea behind a miniaturized antenna is to switch the operating frequency

using MK-DGS from 13.1 GHz to 5 GHz without changing the size of the lateral antenna. At 5 GHz, a directivity of 3.58 dBi was increased to 7.95 dBi by using an MTM superstrate at a height of 17 mm, while the gain is increased from 3.15 dBi to 7.8 dBi. The relationship between the proposed miniaturized antenna and certain DGS-based works is shown in Table 1.

Table 1. A comparison of the previous work using DGS.

Ref	size (mm^2)	Miniaturization (%)	Switching resonance Frequency [GHz]		Application
			Before switch	**After switch**	
[14]	$0.28\lambda_0 * 0.28\lambda_0$	56.89	5.8	2.5	ISM
[15]	$0.22\lambda_0 * 0.29\lambda_0$	57.77	5.8	2.45	ISM
[16]	$0.31\lambda_0 * 0.34\lambda_0$	65.0	10	3.5	WiMAX
[17]	$0.28\lambda_0 * 0.28\lambda_0$	57.77	5.8	2.45	ISM
[18]	$0.21\lambda_0 * 0.19\lambda_0$	27.02	7.4	5.4	ISM
[19]	$0.12\lambda_0 * 0.19\lambda_0$	53.6	5.8	2.69	Arrays
[20]	$0.25\lambda_0 * 0.243\lambda_0$	51.27 and 36.77	14.9	9.42 and 7.26	Wireless data transmission
Proposed	$0.25\lambda_0 * 0.25\lambda_0$	61.83	13.1	5	WLAN

2. MINIATURIZED PENTAGONAL SLOT ANTENNA WITH MEANDER-KOCH DGS

Figures 1(a)–(c) show the top and bottom views of prototype design and configuration for a basic PSA, on an FR4 epoxy substrate with $h_1 = 1.6$ mm thickness and $\varepsilon_{r1} = 4.4$ dielectric constant. The dimensions of its ground plane are $L_g * W_g = 15 * 15$ mm^2 and it operates in Ku-band at 13.1 GHz. The mathematical Equations (1) and (2) represent the 50 ohm feeder length (L_f) and characteristic impedance (Z_0) of a microstrip line [22], respectively.

$$Z_0 = \frac{377}{\sqrt{\varepsilon_r \left(\frac{w}{h} + 1.393 + 0.667\ln\left(\frac{w_f}{h} + 1.444\right)\right)}} \tag{1}$$

$$L_f = \frac{L_{\lambda/4}}{\pi} \cos^{-1}\sqrt{\frac{50}{z_0}} \tag{2}$$
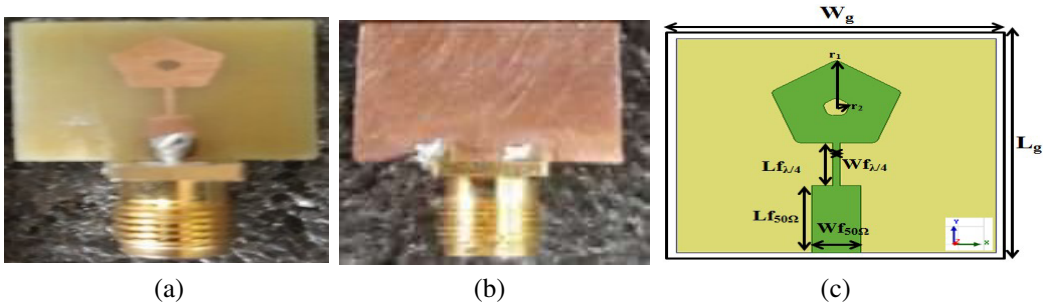

(a)   (b)   (c)

Figure 1. Prototype model. (a) Top view, (b) back view and (c) pentagonal slot antenna configuration.
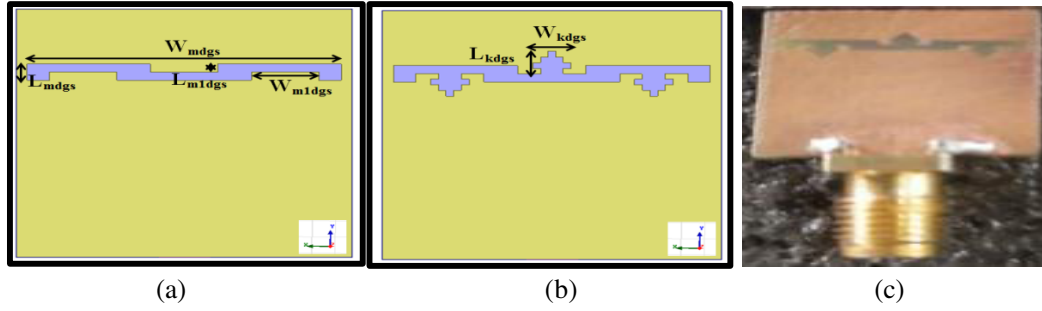
Figure 2. Steps involved in designing a proposed antenna using Meander Koch DGS: (a) Meander, (b) Koch structure, (c) prototype model of combination of Meander Koch DGS.

A fillet radius 0.3 mm is used to smooth the edge of the vertices of a pentagonal slot antenna with $r_1 = 3.1$ mm and $r_2 = 0.6$ mm. A miniaturized PSA with MK-DGS has been designed and fabricated in Figures 2(a)–(c). The steps involved in designing the proposed antenna use a meander DGS and Koch technique where slots are loaded at the periphery of the meander, respectively. According to the DGS principle, defects engraved on the ground plane can be periodic or aperiodic. The DGS is characterized by disrupted current distribution on the ground plane, which changes the values of line inductance and capacitance, thereby varying current flow and input impedances [14]. As a result, the antenna has been 61.83% miniaturized with optimized parameter values shown in Table 2, close to an electrically small antenna capable of switching from 13.1 GHz to 5 GHz. The proposed miniaturized PSA with MK-DGS was intended to approach the Chu-limit in Equation (3). An antenna is surrounded by a sphere 'a'.

$$Q_{chu} = \frac{1}{ka} + \frac{1}{(ka)^3} \tag{3}$$

In [3] by McLean, a numerical relationship was proposed between the distribution of the source and its corresponding inside the sphere of antenna configuration. A sphere with a radius of 7.5 mm is used for calculation of the Chu-limit [3] for a miniaturized PSA loaded with MK-DGS. A Koch curve is divided into n segments, Consider $W_{m1dgs} = L$ Euclidian segments. A method for dividing a line segment is shown in Figures 2(d)–(g). An identical structure is used in all iterations to replace the middle segment. Each iteration increased the length of each line to 5/3rd of the original. As shown in Equation (4), the new length is L_n (4)

$$L_n = L(5/3)^n \tag{4}$$

The original line length is L, and the new line length after (n) iterations is L_n. The proposed antenna has a number of iterations of $n = 2$.

Table 2. All of the optimized geometrical dimensions of the proposed antenna.

Parameters	r_1	r_2	$Wf_{50\Omega}$	$Lf_{50\Omega}$	$Lf_{\lambda/4}$	l	b_e	L_{mdgs}	W_{mdgs}	W_{m1dgs}	L_{m1dgs}	L_{kdgs}	W_{kdgs}	w_{strip}	$Wf_{\lambda/4}$
Optimized Value [mm]	3.1	0.6	2.3	4.7	3.2	5.2	2.65	14.1	1	3	0.5	1	1	0.25	0.38

Figures 3(a)–(b) show the measured and simulated S_{11} characteristics of a basic pentagonal slot antenna, and MK-DGS loaded. The basic PSA was initially designed at 13.1 GHz with a return loss of -31.67 dB. The final design and fabricated basic PSA with a meander Koch DGS operates at 5 GHz with a return loss of -27.2 dB.

Figure 3(c) depicts the parametric analysis of meander DGS with different widths. By increasing widths of meander DGS 'W_{m1dgs}' and 'W_{mdgs}', resonant frequency shifts to lower frequency (from right
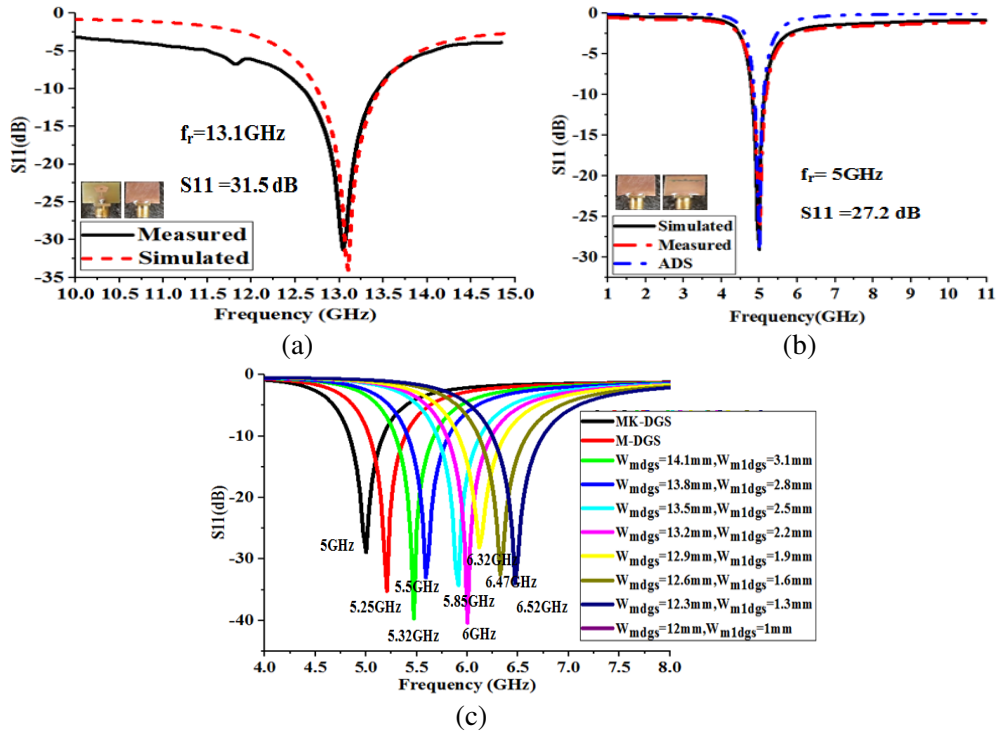
Figure 3. The measured and simulated characteristics of return loss of (a) PSA, (b) PSA functionalized with meander-Koch DGS technique and (c) different width of 'W_{m1dgs}' and 'W_{mdgs}'.

to left). Basic PSAs loaded with and without MK-DGS operating at 13.1 GHz and at 5 GHz respectively are shown in Figures 4(a) and (b) in the E ($\phi = 0°$) and H ($\phi = 90°$). Radiation can be observed omnidirectional on the H-plane at 5 GHz whereas on the E-plane at the same frequency, it exhibits a selective dumbbell-shaped partial pattern. Table 3 compares the characteristics of miniaturized antenna and basic PSA, respectively. Figure 5 shows the Patch Antenna Circuit Section (PACS) connected to the DGS Circuit Section (DGSCS) via a pairing component between the ground plane and patch.

Table 3. Characteristics of miniaturized antenna.

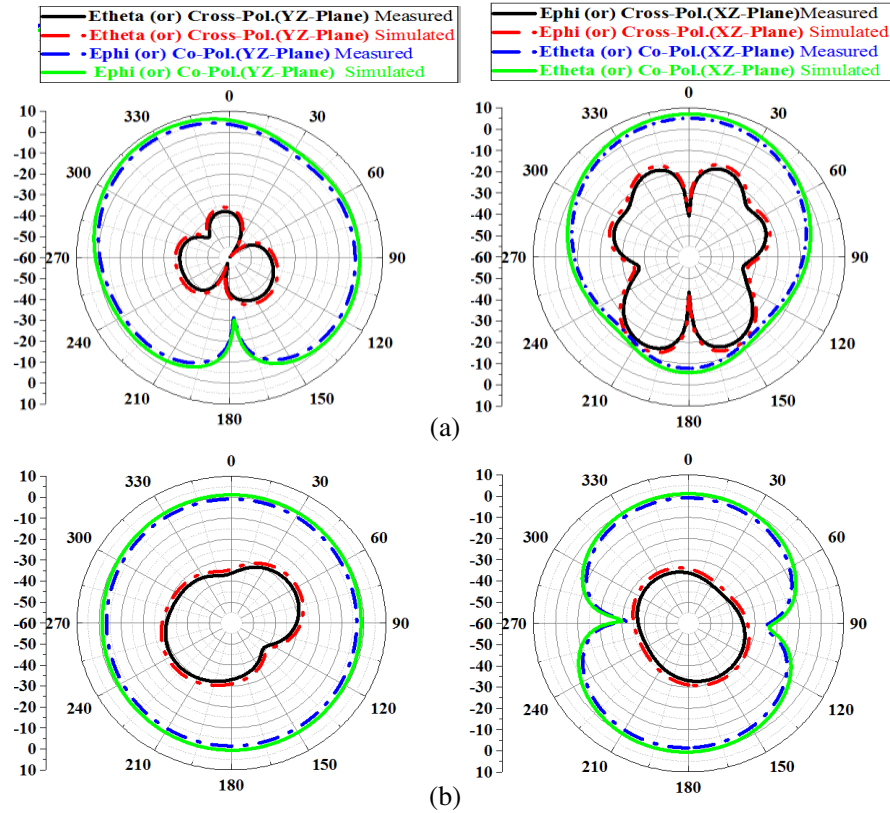| Parameter	Basic PSA	Miniaturized PSA with MK-DGS loaded	Miniaturized PSA with MM loaded
Resonant freq. (GHz)	13.1	5	5
Ka and Q_{chu}	2.14, 0.55	0.78, 3.38	X
Gain (dBi)	6.20	3.15	7.8
Bandwidth (GHz)	0.73	0.33	0.37
Directivity (dBi)	7.46	3.58	7.95
Efficiency (%)	92.2	43.23	79.83
E-pol X-pol (dB)	−33.20	−33.20	−38.5
H-pol X-pol (dB)	−24.52	−16.35	−25.02

X: Not mentioned

Figure 4. Radiation patterns of measured and simulated for (a) basic PSA at 13.1 GHz, and (b) miniaturized antenna at 5 GHz.
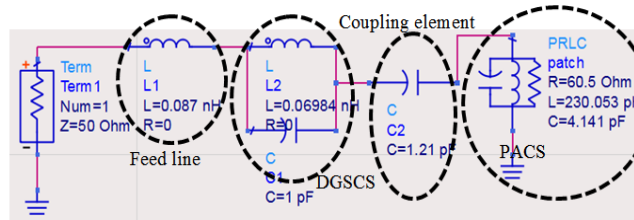

Figure 5. Miniaturized PSA using MK-DGS equivalent circuit model.

3. MINIATURIZED PSA CHARACTERISTICS WITH GAIN ENHANCEMENT

The MTM superstrate is introduced in this section, which increases the miniaturized antenna performance from the previous section. An artificial dielectric superstrate has been used to increase the power density radiated on broadside of a miniaturized antenna. The electric field is parallel to the surface of the unit cell when the wave vector 'k' is normal to the surface. Because of this, the unit cell must be etched on either side of the substrate. On the Rogers RT Duroid 5880 substrate a 2×2 metamaterial matrix was on one side and four metallic strip lines on the other. Figure 6(a) depicts the unit cell MTM structure simulation setup with $a_x = 6$ mm, $a_y = 6$ mm, and $a_z = 6$ mm.

The proposed MTM unit cell structure is shown in Figure 6(b). The capacitance gaps C_{gap1}, C_{gap2} and series capacitances C_{s1}, C_{s2} are represented by the electric field intensity curve in Figure 6(c). A distribution of surface current curve for strip inductance (L_{strip}) and metallic ring inductance (L_{Total}) is shown in Figure 6(d). The unit cell of MTM equivalent circuit is represented in Figures 7(a) and (b) by the equivalent circuit where the metallic rings are associated with an inductance L_{Total} that is parallel to C_{eq}. The strip can exist because of the inductance L_{strip}.
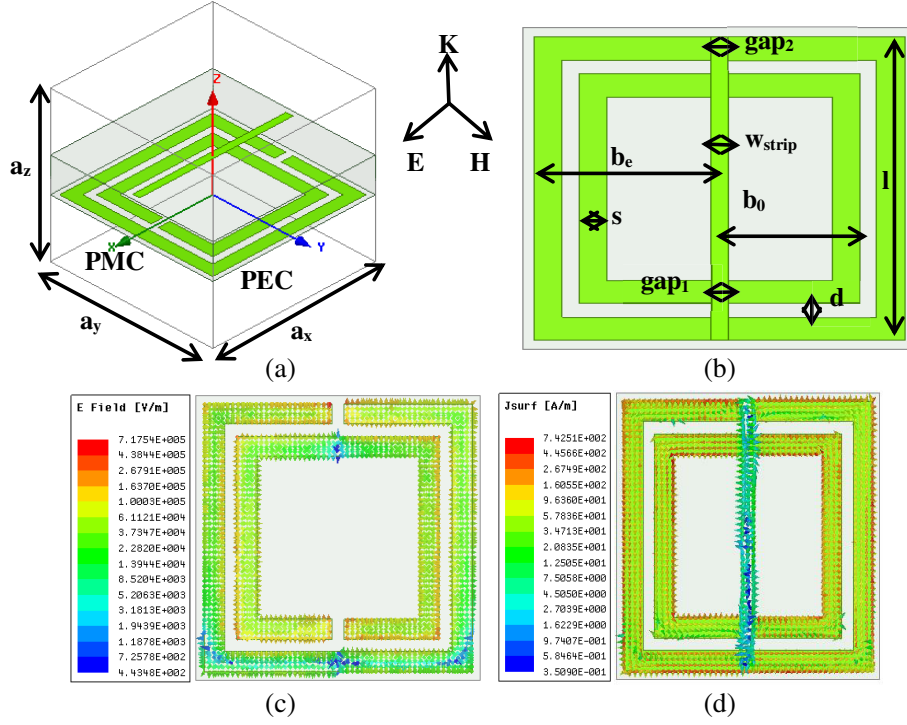
Figure 6. (a) MTM unit cell setup for simulation, (b) MTM unit cell, (c) electric field intensity, and (d) distribution of surface current at 5 GHz.
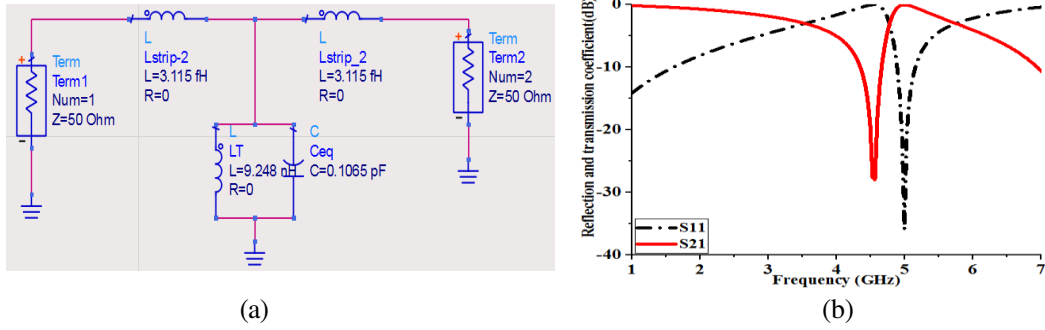

Figure 7. (a) Circuit of a unit cell with an approximate T-equivalent, (b) parameters S_{11} and S_{21} retrieved from HFSS.

The unit cells of MTM have their resonant frequency f_r which is given by:

$$f_r = \frac{1}{2\pi}\sqrt{\frac{1}{C_{eq}\left(L_{strip} + L_{Total}\right)}} \tag{5}$$

The total equivalent inductance L_{Total} for a rectangular cross section wire with finite length l_f and width s can be calculated using Equations (6) and (7) [23–25].

$$l_f = 8b_e - g \tag{6}$$

$$L_{Total} = 0.0002l_f\left(2.303\log_{10}\frac{4l_f}{s} - \gamma\right)\mu H \tag{7}$$

The average ring dimension is b_{avg} expressed as:

$$C_s = C_{s1} = C_{s2} = \left(4b_{avg} - g\right)C_{pul} \tag{8}$$

where,

$$b_{avg} = b_e - s - \frac{d}{2} \text{ and } C_{pul} = \frac{\sqrt{\varepsilon_{eff}}}{CZ_0} \tag{9}$$

An inductance of the strip L_{strip} is given as

$$L_{strip}(\text{nH}) = 2 \times 10^{-4} l \left[\ln\left(\frac{l}{w_{strip} + t}\right) + 1.193 + \frac{w_{strip} + t}{3l} \right] \cdot K_g \tag{10}$$

The unit cell of MTM is computed as $L_{strip} = 6.230\,\text{fH}$, $C_{eq} = 0.1065\,\text{pF}$, $L_{Total} = 9.28\,\text{nH}$, and $f_r = 5.05\,\text{GHz}$ from Equations (8) to (11). Table 4 compares simulated and calculated resonant frequencies for various aspects of an MTM unit cell.

Table 4. Comparison of simulated and calculated resonant frequencies for different values b_e of a MTM unit cell. $t = 0.035\,\text{mm}$, $\varepsilon_{r2} = 2.2$, $h_2 = 1.575\,\text{mm}$, $s = 0.5\,\text{mm}$, $d = 0.25\,\text{mm}$.

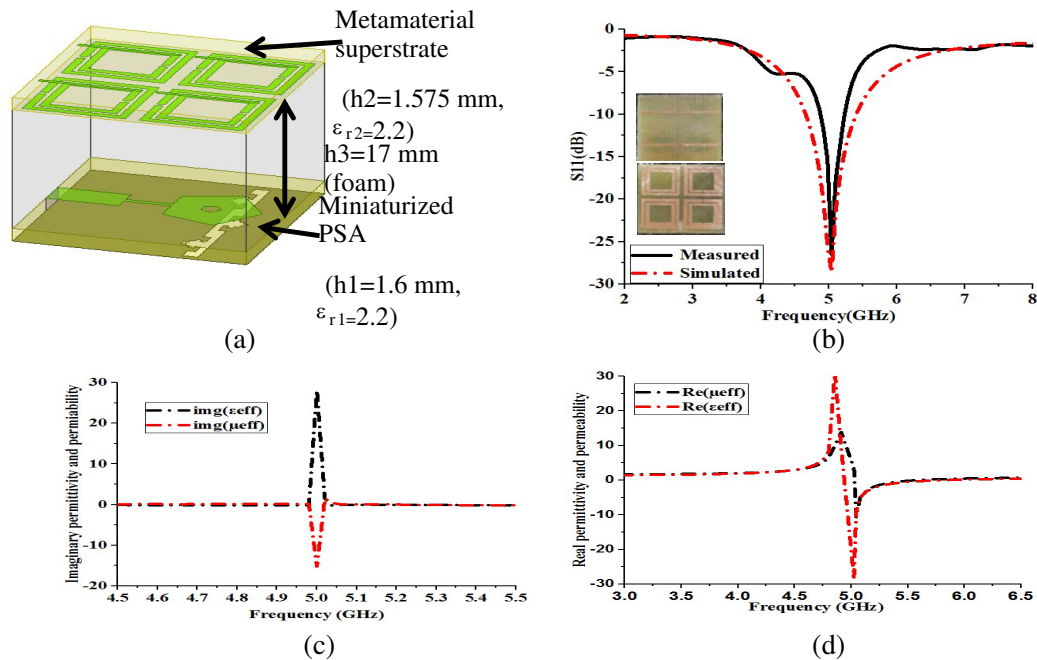| L_{Total} (nH)	b_e (mm)	Resonance Frequency f_r [GHz]		b_{avg} (mm)	C_{pul} (pF)
		Simulated	Computed		
8.737	2.3	6.19	6.35	1.675	25.33
8.915	2.4	5.73	5.97	1.775	26.10
9.032	2.5	5.49	5.57	1.875	27.62
9.248	2.6	5.01	5.05	1.975	30.79
9.356	2.7	4.74	4.85	2.075	31.73
9.434	2.8	4.42	4.51	2.175	34.29
9.657	2.9	4.13	4.32	2.275	35.31
9.799	3.0	3.90	3.95	2.375	37.90

Figure 8. (a) A basic PSA with MK-DGS and MTM superstrate loaded, (b) return loss of proposed antenna, (c) imaginary, and (d) real values of ε_{eff} and μ_{eff}.
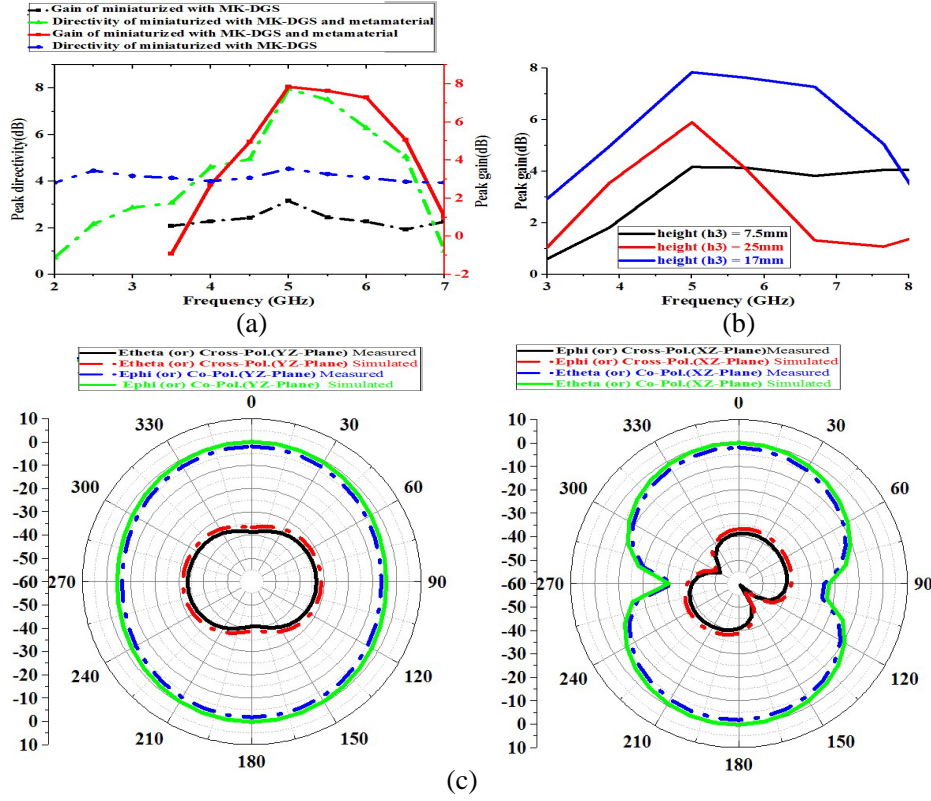
Figure 9. (a) Peak directivity peak gain VS frequency, (b) peak gain with different the height (h_3) of the MTM superstrate, and (c) radiation patterns of proposed antenna.

Figure 8(a) shows the final antenna MTM setup with foam height of 17 mm. Figures 8(b)–(c) represent the values of ε_{eff} and μ_{eff} at 5 GHz. The miniaturized antenna peak gain has been enhanced from 3.15 dB to 7.84 dB whereas the peak directivity is enhanced from 3.58 dB to 7.95 dB at 5 GHz, as shown in Figure 9(a). The MTM superstrate shown in Figure 9(b) was subjected to parametric analysis by changing its height (h_3). At 5 GHz, a maximum peak gain of 7.84 dB was achieved at height (h_3) = 17 mm (approximately $\lambda/4$). Figure 9(c) illustrates the radiation patterns in the H ($\phi = 90°$) and E ($\phi = 0°$) planes of basic PSA with MK-DGS and MTM superstrate loaded operating at 5 GHz.

Table 5. Comparing proposed antenna with smallest lateral antenna size, and enhanced parameters with the other structures.

Parameter Ref.	Ground plane size (mm)^2	Vertical antenna Size (mm)	Lateral antenna Size (mm^2)	Resonant frequency (GHz)	Efficiency (%)	Gain (dBi)	Directivity (dBi)
[26]	$0.272\lambda_0 * 0.272\lambda_0$	$0.024\lambda_0$	$0.099\lambda_0 * 0.153\lambda_0$	2.40	25.5	-2.02	3.91
[27]	$0.139\lambda_0 * 0.139\lambda_0$	$0.0146\lambda_0$	$0.10\lambda_0 * 0.10\lambda_0$	1.90	48.2	-1.22	1.95
[28]	$0.196\lambda_0 * 0.196\lambda_0$	$0.019\lambda_0$	$0.098\lambda_0 * 0.098\lambda_0$	2.45	28.1	-1.28	4.23
[29]	$0.36\lambda_0 * 0.36\lambda_0$	$0.0142\lambda_0$	$0.253\lambda_0 * 0.253\lambda_0$	2.5/4.5/5.9	72/78/70	3.5/4.5/4.2	X
[30]	$0.304\lambda_0 * 0.115\lambda_0$	$0.2845\lambda_0$	$0.0341\lambda_0 * 0.0360\lambda_0$	1.575	60	4.85	5
Current work	$0.25\lambda_0 \times 0.25\lambda_0$	$0.3361\lambda_0$	$0.0516\lambda_0$	5	79.83	7.84	7.95

X: Not mentioned

The performance of the proposed antenna structure is compared to that of other planar antennas in the literature in Table 5. The proposed antenna has a higher gain, directivity, bandwidth, and smaller lateral antenna size than the other structures.

$$\mu = \eta \times z \text{ and } \varepsilon = \frac{\eta}{z} \tag{11}$$

where,

$$\eta = \frac{1}{kd} \cos^{-1} \left[\frac{1}{2S_{21}} \left(1 - S_{11}^2 + S_{21}^2 \right) \right] \text{ and } z = \sqrt{\frac{(1 + S_{11})^2 - S_{21}^2}{(1 - S_{11})^2 - S_{21}^2}} \tag{12}$$

4. CONCLUSION

The design of a 5 GHz WLAN basic PSA with MK-DGS and MTM based superstrate is presented. An antenna loaded with MK-DGS has a resonant frequency reduced from 13.1 GHz to 5 GHz because of a 61.83% miniaturization, leading to the enhancement of antenna bandwidth, efficiency, directivity, and gain. The MTM superstrate is designed over a basic PSA loaded with MK-DGS, gain increased from 3.15 to 7.84 dBi, and directivity increased from 3.58 dB to 7.95 dBi at 5.2 GHz. Permittivity and permeability are calculated by retrieving the parameter values of a square MTM unit cell. Experiments are performed on a prototype model of the antenna, and exact relationships are observed.

REFERENCES

1. Fallahpour, M. and R. Zoughi, "Antenna miniaturization techniques: A review of topology- and material-based methods," *IEEE Antennas and Propagation Magazine*, Vol. 60, No. 1, 38–50, Feb. 2018.

2. Chu, L. J., "Physical limitations of omni-directional antennas," *Journal of Applied Physics*, Vol. 19, No. 12, 1163–1175, 1948.

3. McLean, J. S., "A re-examination of the fundamental limits on the radiation Q of electrically small antennas," *IEEE Transactions on Antennas and Propagation*, Vol. 44, 672–676, May 1996.

4. Erentok, A. and R. W. Ziolkowski, "Metamaterial-inspired efficient electrically small antennas," *IEEE Transactions on Antennas and Propagation*, Vol. 56, No. 3, 691–707, 2008.

5. Jahani, S., J. Rashed-Mohassel, and M. Shahabadi, "Miniaturization of circular patch antennas using MNG metamaterials," *IEEE Antennas and Wireless Propagation Letters*, Vol. 9, 1194–1196, 2010.

6. Tang, M. and R. W. Ziolkowski, "A study of low-profile, broadside radiation, efficient, electrically small antennas based on complementary split ring resonators," *IEEE Transactions on Antennas and Propagation*, Vol. 61, No. 9, 4419–4430, Sept. 2013.

7. Ghosh, B., S. M. Haque, and D. Mitra, "Miniaturization of slot antennas using slit and strip loading," *IEEE Transactions on Antennas and Propagation*, Vol. 59, No. 10, 3922–3927, Oct. 2011.

8. Ghosh, B., S. K. M. Haque, and N. R. Yenduri, "Miniaturization of slot antennas using wire loading," *IEEE Antennas and Wireless Propagation Letters*, Vol. 12, 488–491, 2013.

9. Ghosh, B., S. M. Haque, D. Mitra, and S. Ghosh, "A loop loading technique for the miniaturization of non-planar and planar antennas," *IEEE Transactions on Antennas and Propagation*, Vol. 58, No. 6, 2116–2121, Jun. 2010.

10. Ramzan, M. and K. Topalli, "A miniaturized patch antenna by using a CSRR loading plane," *International Journal of Antennas and Propagation*, Vol. 2015, 1–9, 2015.

11. Sedghi, M. S., M. Naser-Moghadasi, and F. B. Zarrabi, "Microstrip antenna miniaturization with fractal EBG and SRR loads for linear and circular polarizations," *International Journal of Microwave and Wireless Technologies*, Vol. 9, No. 4, 891–901, May 2017.

12. Reddy, G. B., M. H. Adhithya, and D. S. Kumar, "Miniaturization of microstrip slot antenna using high refractive index metamaterial based on single ring split ring resonator," *Progress In Electromagnetics Research Letters*, Vol. 93, 115–122, 2020.

13. Mishra, N. and R. K. Chaudhary, "A miniaturized directive high gain metamaterial antenna using ELC ground for WiMAX application," *International Journal of Electronics Letters*, Vol. 7, No. 1, 68–76, 2019.

14. Er-Rebyiy, R., J. Zbitou, M. Latrach, A. Tajmouati, A. Errkik, and L. El Abdellaoui, "New miniature planar microstrip antenna using DGS for ISM applications," *TELKOMNIKA*, Vol. 15, No. 3, 1149–1154, Sept. 2017.

15. Ghaloua, A., J. Zbitou, L. El Abdellaoui, and M. Latrach, "A miniature circular patch antenna using defected ground structure for ISM band applications," *ICCWCS'17*, Article No. 82, 1–5, Larache, Morocco, Nov. 14–16, 2017.

16. Er-Rebyiy, R., J. Zbitou, M. Latrach, A. Tajmouati, A. Errkik, and L. El Abdellaoui, "A novel design of a miniature low cost planar antenna for ISM band applications," *ICCWCS'17*, Article No. 6, 1–5, Larache, Morocco, Nov. 14–16, 2017.

17. Mouhssine, A., Z. Doulfakar, R. Dakir, A. Erkkik, and M. Latrach, "A new compact and miniaturized CPW antenna with DGS and paper substrate for ISM band applications," *ICCWCS'17*, Article No. 78, 1–6, Larache, Morocco, Nov. 14–16, 2017.

18. Er-Rebyiy, R., J. Zbitou, A. Tajmouati, M. Latrach, A. Errkik, and L. El Abdellaoui, "A new design of a miniature microstrip patch antenna using defected ground structure DGS," *2017 International Conference on Wireless Technologies, Embedded and Intelligent Systems (WITS)*, 1–4, 2017.

19. Ghaloua, A., L. El Abdellaoui, L. El Abdellaoui, M. Latrach, A. Tajmouati, and A. Errkik, "A novel configuration of a miniature printed antenna array based on defected ground structure," *International Journal of Intelligent Engineering and Systems*, Vol. 12, No. 1, 211–220, 2019.

20. Swetha, A. and K. R. Naidu, "Miniaturized antenna using DGS and meander structure for dual-band application," *Microwave and Optical Technology Letters*, Vol. 62, No. 11, 3556–3563, 2020.

21. Mitra, D., B. Ghosh, A. Sarkhel, and S. R. B. Chaudhuri, "A miniaturized ring slot antenna design with enhanced radiation characteristics," *IEEE Transactions on Antennas and Propagation*, Vol. 64, No. 1, 300–305, 2016.

22. Huang, Y. and K. Boyle, *Antennas from Theory to Practice*, John Wiley & Sons Ltd., UK, 2008.

23. Terman, F. E., "Network theory, filters, and equalizers," *Proceedings of the IRE*, Vol. 31, No. 6, 288–302, 1943.

24. Bahl, I. J. and P. Bhartia, *Microwave Solid State Circuit Design*, 26-0947, 1988.

25. Numan, A. B. and M. S. Sharawi, "Extraction of material parameters for metamaterials using a full-wave simulator," *IEEE Antennas and Propagation Magazine*, Vol. 55, No. 5, 202–211, 2013.

26. Dong, Y., H. Toyao, and T. Itoh, "Design and characterization of miniaturized patch antennas loaded with complementary split-ring resonators," *IEEE Transactions on Antennas and Propagation*, Vol. 60, No. 2, 772–785, 2012.

27. Mitra, D., B. Ghosh, A. Sarkhel, and S. R. B. Chaudhuri, "A miniaturized ring slot antenna design with enhanced radiation characteristics," *IEEE Transactions on Antennas and Propagation*, Vol. 64, No. 1, 300–305, 2016.

28. Ouedraogo, R. O., E. J. Rothwell, A. R. Diaz, K. Fuchi, and A. Temme, "Miniaturization of patch antennas using a metamaterial-inspired technique," *IEEE Transactions on Antennas and Propagation*, Vol. 60, No. 5, 2175–2182, 2012.

29. Varamini, G., A. Keshtkar, and M. Naser-Moghadasi, "Miniaturization of microstrip loop antenna for wireless applications based on metamaterial metasurface," *AEU — International Journal of Electronics and Communications*, Vol. 83, 32–39, 2018.

30. Suvarna, K., N. Ramamurthy, and D. V. Vardhan, "Miniaturized and gain enhancement of tapered patch antenna using defected ground structure and metamaterial superstrate for GPS applications," *Progress In Electromagnetics Research C*, Vol. 108, 187–200, 2021.